Talanta 108 (2013) 150–156

Contents lists available at SciVerse ScienceDirect

Talanta

journal homepage: www.elsevier.com/locate/talanta

C_2-symmetrical hexaazatriphenylene derivatives as colorimetric and ratiometric fluorescence chemsensors for Zn^{2+}

Xiao-Hong Zhang, Qiang Zhao, Xiu-Ming Liu, Tong-Liang Hu, Jie Han*, Wen-Juan Ruan*, Xian-He Bu

Department of Chemistry and Tianjin Key Laboratory on Metal and Molecule-based Material Chemistry, Nankai University, No. 94, Weijin Road, Tianjin 300071, PR China

ARTICLE INFO

Article history:
Received 18 December 2012
Received in revised form
21 February 2013
Accepted 27 February 2013
Available online 7 March 2013

Keywords:
C_2-symmetrical hexaazatriphenylene
Colorimetric
Ratiometric
Chemsensor
Zinc ion

ABSTRACT

Two C_2-symmetrical hexaazatriphenylene (HAT) derivatives, 2,3-diphenyl-6,7,10,11-tetra(pyridin-2-yl)dipyrazino[2,3-f:2′,3′-h]quinoxaline (**1**) and 2,3,6,7-tetraphenyl-10,11-di(pyridin-2-yl)dipyrazino[2,3-f:2′,3′-h]quinoxaline (**2**), were designed and synthesized by the condensation reaction of 1,2-diamines and 1,2-diketones. Both compounds **1** and **2** exhibit sensitive, ratiometric and colorimetric fluorescence selectivity for Zn^{2+} ion over alkali ions, alkaline earth ions and a wide range of transition metal ions upon excitation at 350 nm in acetonitrile/water. The interactions between **1** or **2** and Zn^{2+} can be observed by naked eyes with an obvious color change of the solution from colorless to yellow. For fluorescence intensity of **2** toward Zn^{2+}, a good linearity (correlation coefficient $R^2=0.993$) was established with a detection limit of 0.095 μM, which is more sensitive than that of **1** (0.2 μM). The binding modes of the free ligands **1** and **2** with Zn^{2+} are discussed in context to their photophysical and electrochemical properties as well as single X-ray crystallographic structures of **1**, **2** and **1**-Zn.

1. Introduction

Hexaazatriphenylene (HAT) and its derivatives, based on the variety of structures readily modified by their six substituent groups, have received intense attention in view of their applications to develop n-type semiconductors [1,2], liquid crystals [3,4], magnetic materials [5–7], ligands for coordination chemistry [8–10] and self-assembly morphologies [11–13]. Because of the symmetrical array of three chelating sites to metal ions, HAT derivatives which are disk-shaped aromatic molecules have been used in construction of attractive metal-assembled systems [14,15]. Furthermore, the HAT derivatives can also be developed as selective fluorescence sensors for metal ions in environmental monitoring, although the investigations of the HATs on application for fluorescence chemsensors are just at the initial stage. Recently, the first fluorescence chemsensor of HATs, hexa-2-pyridyl hexaazatriphenylene (HPDQ), was synthesized by merging six pyridine units into a HAT core [11], which showed highly on/off fluorescence selectivity for Cd^{2+} over many other metal ions [16]. Inspired by the pioneering work above, it is valuable to design a series of HAT derivatives with different coordination structures, such as non-centrosymmetric HATs which are still quite rare mainly due to the lack of practical synthesis methods [17–19], in order to obtain different fluorescence sensors for different metal ions. Additionally, to the best of our knowledge, non-centrosymmetric HAT-based fluorescence chemsensors for selective recognition of transition metal ions have not ever been reported in literatures.

Zinc, as the second most abundant transition metal in the human body, plays diverse roles in biological activities such as catalytic cofactors and neural signal transmitters [20–22]. Although much research of fluorescence chemsensors for Zn^{2+} has been carried out, the development of highly sensitive selective ratiometric and fluorescence chemosensors for zinc ions is still an important task in science and technology [23,24]. Herein, two novel C_2-symmetrical HAT compounds, 2,3-diphenyl-6,7,10,11-tetra(pyridin-2-yl)dipyrazino[2,3-f:2′,3′-h]quinoxaline (**1**) and 2,3,6,7-tetraphenyl-10,11-di(pyridin-2-yl)dipyrazino[2,3-f:2′,3′-h]quinoxaline (**2**), bearing different number of pyridine groups were designed and synthesized conveniently by two step reactions (see Scheme 1). The two C_2-symmetrical HAT compounds **1** and **2** are architecturally different in their coordination geometry compared with the symmetrical HPDQ [11]. That is to say, HPDQ has three identical chelating sites and each site has four N atoms, while **1** and **2** exhibit two different types of binding sites with different N atoms, which lead to selectivity for other metal ions rather than Cd^{2+}. Both **1** and **2** exhibit ratiometric and colorimetric fluorescence recognition of Zn^{2+} nearly without interference by many other background metal ions, including alkali ions, alkaline earth ions and a wide range of transition metal ions. The selective recognition behaviors for Zn^{2+} are

* Corresponding authors. Tel.: +86 22 23498361, +86 22 23501717; fax: +86 22 23502458.
E-mail addresses: hanjie@nankai.edu.cn (J. Han), wjruan@nankai.edu.cn (W.-J. Ruan).

0039-9140/$ - see front matter © 2013 Elsevier B.V. All rights reserved.
http://dx.doi.org/10.1016/j.talanta.2013.02.071

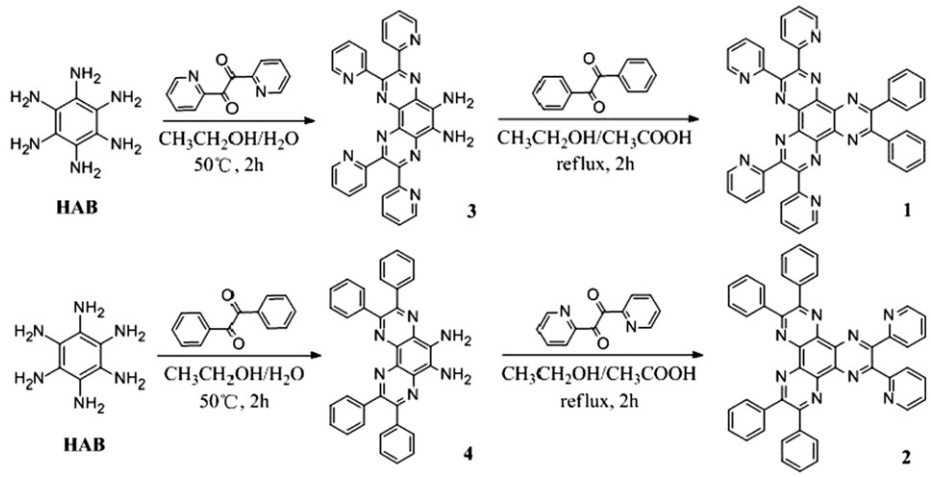

Scheme 1. Synthesis routes of **1** and **2** .

discussed according to the photophysical and electrochemical properties of free ligands as well as single X-ray crystallographic structures of **1**, **2** and **1**-Zn.

2. Experimental

2.1. Materials and general methods

All reagents and chemicals were purchased from commercial sources and were used as received unless stated otherwise. All solvents used for photophysical studies were purified by standard procedures. The ^{1}H NMR spectrum was measured in $CDCl_3$ with a Bruker 400 MHz NMR spectrometer with chemical shifts reported as ppm. Elemental analyses (C, H, and N) were tested using a Perkin-Elmer 240C analyzer. IR spectra were obtained on a TENSOR 27 OPUS Fourier transform infrared (FT-IR) spectrometer (Bruker) using KBr disks dispersed with sample powders in the 4000–400 cm^{-1} range. UV–vis absorption spectra were recorded on a Shimadzu UV-2450 spectrophotometer and fluorescence spectra were recorded on a Varian Cary Eclipse fluorescence spectrometer. Mass spectra were carried out in a TRACE DSQ spectrometer.

2.2. Synthesis of 2,3-diphenyl-6,7,10,11-tetra(pyridin-2-yl)-dipyrazino[2,3-f:2′,3′-h]quinoxaline (*1*)

The synthesis routes of the target HAT derivatives are outlined in Scheme 1. Compound hexaaminobenzene (HAB) was prepared according to the literature methods [25,26]. HAB (1 g, 5.9 mmol) dissolved in a mixture of water (75 mL) and ethanol (220 mL) under nitrogen atmosphere, and the solution was heated to 50 °C for 10 min. Then a solution of 2,2′-pyridil (2.5 g, 11.9 mmol) in ethanol (75 mL) was added dropwise. The reaction mixture was stirred for 2 h and then allowed to cool down to room temperature. The solid product diamine (**3**) was filtered and washed with ethanol, which was used directly in the next reaction step. Under nitrogen atmosphere benzil (84 mg, 0.4 mmol) and **3** (202 mg, 0.4 mmol) were added to a mixture of ethanol (50 mL) and acetic acid (5 mL) and refluxed for 2 h. The precipitation was filtered and purified by column chromatography (silica gel) using dichloromethane/methanol (50/1) as eluent to afford **1** as white solids with yield of 21%. ^{1}H NMR (400 MHz, $CDCl_3$): δ 8.44 (t, J=7.5 Hz, 4H), 8.37 (s, 4H), 7.96 (t, J=7.2 Hz, 4H), 7.88–7.79 (m, 4H), 7.46–7.36 (m, 6H), 7.34–7.27 (m, 4H). MS (ESI-MS) m/z: 695.4 $[M+H]^+$. Anal. calcd. for $C_{44}H_{26}N_{10}\cdot CH_3OH$: C, 74.37%; H, 4.16%; N, 19.27%; Found: C, 74.55%; H, 4.05%; N, 19.01%. IR (KBr, cm^{-1}): 3134, 1585, 1400, 1143, 1093, 1040, 993, 954, 746, 694, 596, and 555.

2.3. Synthesis of 2,3,6,7-tetraphenyl-10,11-di(pyridin-2-yl)-dipyrazino[2,3-f:2′,3′-h]quinoxaline (*2*)

Compound **2** was prepared via a similar procedure to that of **1**. A white solid was obtained with a yield of 22%. ^{1}H NMR (400 MHz, $CDCl_3$) δ 8.46 (d, J=7.6 Hz, 2H), 8.38 (d, J=4.4 Hz, 2H), 7.98 (t, J=7.7 Hz, 2H), 7.89–7.79 (m, 8H), 7.48–7.36 (m, 12H), 7.35–7.29 (m, 2H). MS (ESI-MS) m/z: 693.4 $[M+H]^+$. Anal. calcd. for $C_{46}H_{28}N_8\cdot 2H_2O$: C, 75.81%; H, 4.43%; N, 15.38%; Found: C, 75.93%; H, 4.03%; N, 15.02%. IR (KBr, cm^{-1}): 3132, 1589, 1402, 1369, 1234, 1140, 1040, 951, 772, 696, 596, and 542.

2.4. Growth of the single crystals of *1*, *2* and *1*-Zn

1 or **2** (10 mg) was dissolved in dichloromethane (10 mL) in a test tube. Block-shaped crystals of **1** or **2** were obtained by slow evaporation of the dichloromethane solvent at room temperature for about 2 weeks. **1** (7 mg) dissolved in chloroform (1 mL) in a test tube. A solution of $Zn(NO_3)_2\cdot 6H_2O$ (15 mg) in acetonitrile (10 mL) was added into the tube. Yellow block-shaped crystals **1**-Zn were generated by slow evaporation of the solvent at room temperature for about 3 weeks. Despite extensive efforts, the elemental analyses of **1**-Zn were not well reproduced; this case probably results from the fact that the disorder of the solvent molecules and their extent in the channels may vary depending on the exposure time of the sample to air.

2.5. X-ray data collection and structure determinations

X-ray single-crystal diffraction data for compounds **1**, **2** and **1**-Zn were collected on a SCX-Mini diffractometer at 293(2) K with Mo-Kα radiation (λ=0.71073 Å) by ω scan mode. The program SAINT [27] was used for integration of the diffraction profiles. All the structures were solved by direct methods using the SHELXS program of the SHELXTL package and refined with SHELXL (semi-empirical absorption corrections were applied using SADABS program) [28]. The final refinement was performed by full matrix least-square methods with anisotropic thermal parameters for non-hydrogen atoms on F^2. The hydrogen atoms of the ligands were generated theoretically onto the specific atoms and refined isotropically with fixed thermal factor. CCDC reference numbers are 896264–896266 for **1**-Zn, **1** and **2**, in order.

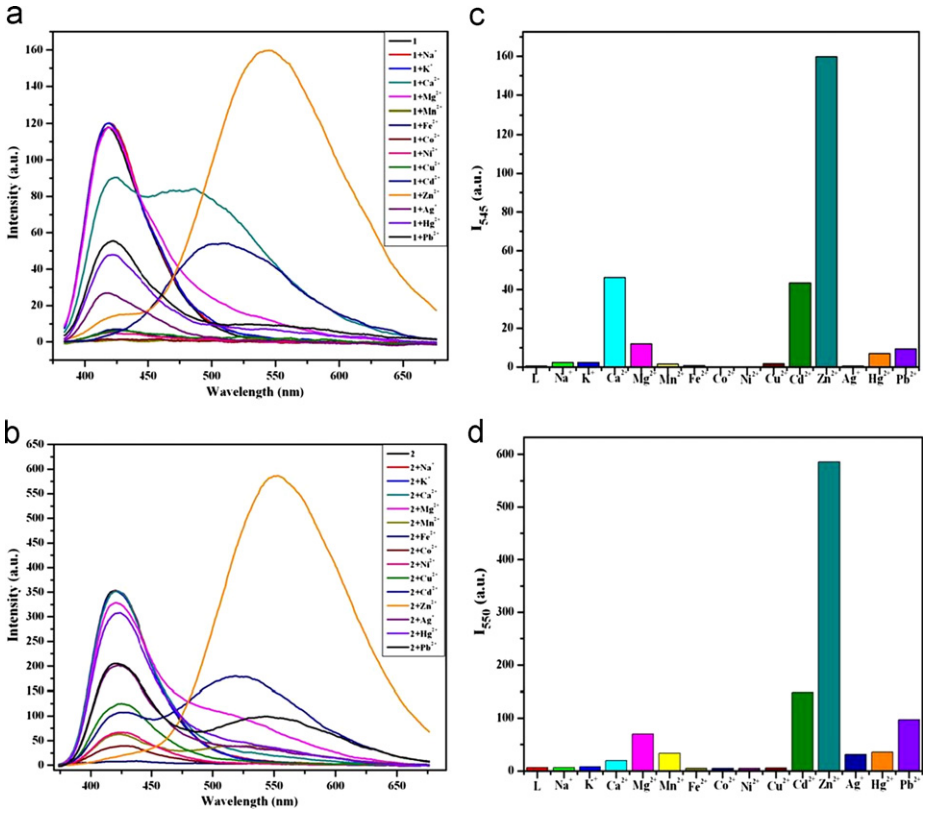

Fig. 1. Fluorescence emission spectra (λ_{ex}=350 nm) of **1** (a) and **2** (b) in the presence of different metal ions (1 equiv) in acetonitrile. Selectivity of **1** (c) at 545 nm and **2** (d) at 550 nm, toward Zn^{2+} and other metal ions (1 equiv). The concentrations of **1** and **2** were respectively 10 μM and 5 μM. The excitation and emission slit widths were 5 nm.

3. Results and discussion

3.1. Fluorescence selectivity for Zn^{2+}

The fluorescence response behaviors of compounds **1** and **2** were investigated by addition of various metal ions (Na^+, K^+, Mg^{2+}, Ca^{2+}, Mn^{2+}, Fe^{2+}, Co^{2+}, Ni^{2+}, Cu^{2+}, Cd^{2+}, Zn^{2+}, Ag^+, Hg^{2+}, and Pb^{2+}) in acetonitrile with the excitation at 350 nm. Upon addition of 1 equiv Zn^{2+} to **1**, significant fluorescence enhancement could be observed with a red-shift band centered at 545 nm, and the fluorescence emission at 417 nm disappeared simultaneously (Fig. 1a). In contrast, the addition of Na^+, K^+, and Mg^{2+} exhibited nearly no effect on the emission spectrum of **1**. Meanwhile, the alkaline earth metal Ca^{2+} and the other transition metal ions Mn^{2+}, Fe^{2+}, Co^{2+}, Ni^{2+}, Cu^{2+}, Ag^+, and Hg^{2+} quenched the emission of **1** to different extents, and a new red-shift band with relatively low intensity appeared upon addition of Ca^{2+} and Cd^{2+}. As shown in Fig. 1c, compared with Zn^{2+}, the fluorescence response caused by the addition of other metal ions to **1** around 545 nm was negligible. In the case of **2**, the addition of Zn^{2+} also led to a pronounced red-shift fluorescence emission centered at 550 nm. The effects by addition of other metal ions to **2** were analogous to those to **1** except Ca^{2+} which exerted no influence on **2** (Fig. 1b). At around 550 nm, the emission caused by the addition of other metal ions to **2** also could be negligible compared with Zn^{2+} (Fig. 1d).

The fluorescence titration experiments were carried out in acetonitrile (Fig. 2a). Upon addition of Zn^{2+} ion to **1**, a gradual decrease in fluorescence intensity at 417 nm and the appearance of a new red-shift emission band at 545 nm were observed simultaneously with an isoemission point at 475 nm, which indicated a clear ratiometric fluorescence change. The ratio of the emission intensity at 417 nm to that at 545 nm (I_{545}/I_{417}) increased from 0.003 to 193.8 upon addition of Zn^{2+}. At the same time, obvious color transformation from colorless to yellow and fluorescence change from blue to bright yellow were also observed (Fig. 2a inset). The fluorescence quantum yield of **1** was 0.007 while that of **1**–Zn^{2+} increased to 0.018 [29]. In the case of **2**, similar fluorescence phenomena were observed as shown in Fig. 2b. After binding Zn^{2+} ion to **2**, the emission band moved red-shifted from 416 to 550 nm and the fluorescence quantum yield increased from 0.015 to 0.092. Apparently, both **1** and **2** present ratiometric and colorimetric fluorescence selectivity for Zn^{2+}. The obvious fluorescence enhancement with red-shift responses may be attributed to two reasons: (1) the coordination of nitrogen atoms to Zn^{2+} ion will reduce the electron with-drawing effect of nitrogen atoms and lower the electron density, which lead to the intramolecular charge-transfer (ICT) effect [16,30–32] and (2) the formation of the metal–complex enhances the plane rigidity, which will be discussed later in crystal structure part, which may increase the conjugated system of the whole molecules [33,34].

We further investigated the fluorescence titration experiment in 5% aqueous acetonitrile, which also showed a ratiometric fluorescence response to Zn^{2+} (Fig. S1). From the theoretical nonlinear fit of experimental data, the logarithm of the binding constant of Zn^{2+} with **1** (log β) is 13.05 ± 0.38, and the binding stoichiometry of **1** to Zn^{2+} is 1:3 (Fig. S2) [35]. Job's plot analysis also proves the 1:3 stoichiometry of **1**–Zn^{2+} (Fig. 3). Furthermore, the ^{1}H NMR titration in $CDCl_3$–CD_3CN (5/1) suggested the formation of stable complex when 3 equiv Zn^{2+} ions were added to the solution of **1**, which also confirmed the 1:3 binding mode of **1**-Zn^{2+} (Fig. S3). With respect to **2**, by the support of nonlinear fit, Job's plot and ^{1}H NMR titration, two Zn^{2+} ions coordinate to one

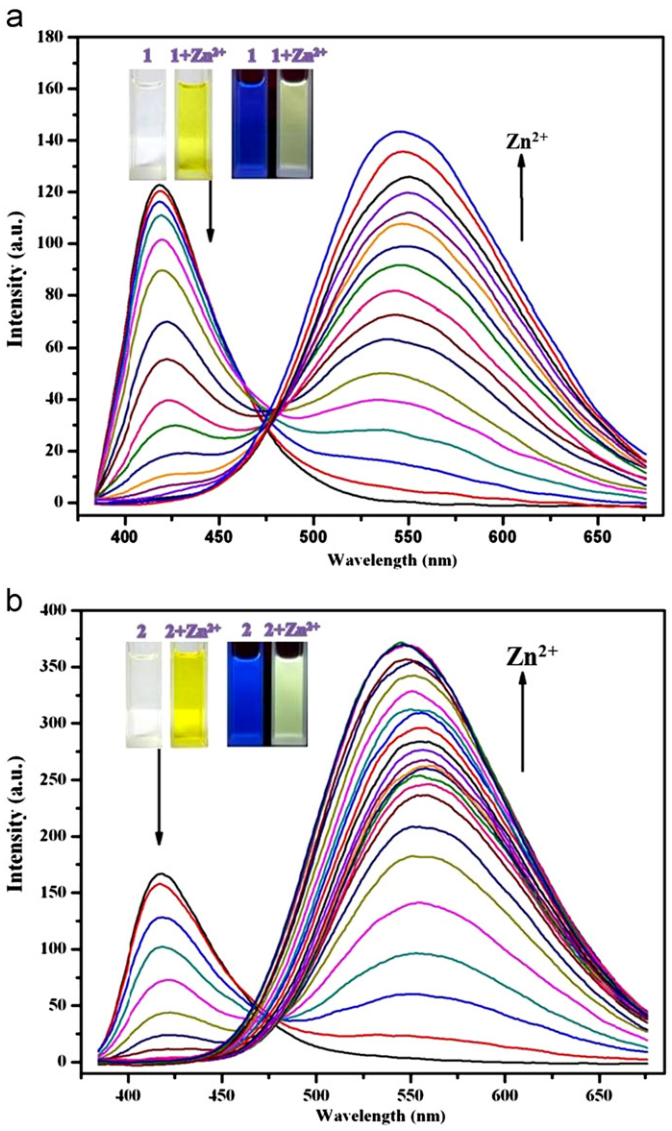

Fig. 2. Fluorescence emission spectra (λ_{ex}=350 nm) of **1** (a) (10 μM) and **2** (b) (5 μM) in acetonitrile upon the addition of Zn^{2+} [(a) 0, 1, 2, 4, 5, 7, 8, 9, 10, 11, 12, 13, 15, 17, 20, 25, 30 μM Zn^{2+}, (b) 0, 0.25, 0.5, 1.0, 1.5, 2.0, 2.5, 3.0, 3.5, 4.0, 4.5, 5.0, 6.0, 7.5, 10, 15, 20, 25, 35, 50, 75, 100, 150, 200, 250 μM Zn^{2+}]. The excitation and emission slit widths were 5 nm. Inset: color changes (left) and fluorescence changes excited by UV lamp (365 nm) (right) in compounds **1** (a) and **2** (b) upon addition of Zn^{2+}.

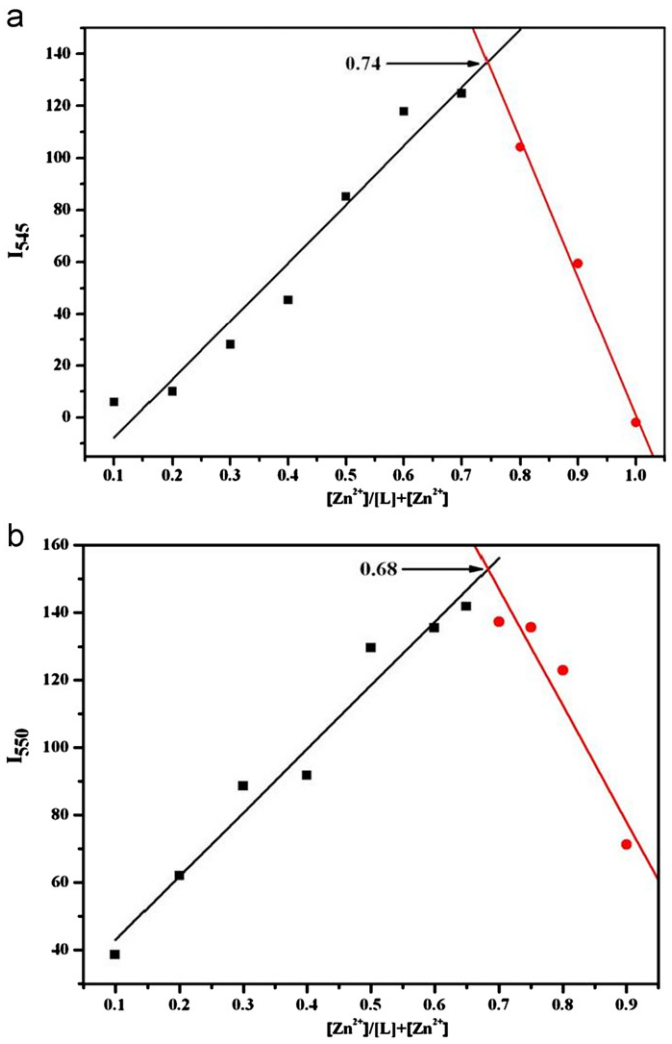

Fig. 3. Job's plot of **1** (a) and **2** (b) to Zn^{2+} in acetonitrile obtained by emission measurements.

molecular **2**. The logarithm of the binding constant of **2**–Zn^{2+} (log β) is 9.6 ± 0.29. Above all, upon addition of Zn^{2+}, **1** forms a trinuclear structure in solution, while a dinuclear structure tends to form between **2** and Zn^{2+}. The proposed coordination modes of **1** and **2** with Zn^{2+} are shown in Fig. 4, which will be discussed in the section of the crystal structures.

Although both **1** and **2** showed good fluorescence selectivity to Zn^{2+} ion, a remarkable difference of the sensitivity in 5% aqueous acetonitrile between **1** (50 μM) and **2** (50 μM) toward Zn^{2+} was observed. The detection limit of **1** was calculated ($3\sigma/k$) in the range of 0–7 μM (R^2=0.991) with a result of 0.2 μM (Fig. S4). The detection limit of **2** toward Zn^{2+} was determined as 0.095 μM by the fluorescence titration data recorded under a concentration range from 0 to 30 μM (R^2=0.993), which was a significant improvement over that observed for **1**. The results suggest that both **1** and **2** are sensitive toward Zn^{2+}, while **2** is much more sensitive than **1**. The main reason for the different sensitivitives between **1** and **2** toward Zn^{2+} may be attributed to the different binding stoichiometries of Zn^{2+} to **1** and **2**. Furthermore, comparing with the existing Zn-sensors [20,35], both **1** and **2** show lower detection limit to Zn^{2+}.

To further evaluate Zn^{2+}-selectivity of **1** and **2** over other metal ions, competition experiments were conducted by addition of 1 equiv of Zn^{2+} ions to the solution of **1** or **2**, respectively, in the presence of 1 equiv of other metal ions. As shown in Fig. S5a, the emission intensity of **1**–Zn^{2+} was nearly unperturbed in the presence of the alkali and alkaline earth ions Na^+, K^+, Mg^{2+} and the heavy transition metal ions Ag^+, Hg^{2+} and Pb^{2+}, while the metal ions Ca^{2+}, Cd^{2+}, Mn^{2+}, Co^{2+} and Ni^{2+}, exhibited an appreciable interference with Zn^{2+}. It is worth to mentioing that Zn^{2+} can be easily detected in the presence of Ca^{2+} although the intensity of **1**–Zn^{2+} is only 3.4-fold that of **1**-Ca^{2+} at 545 nm. Similarly, **2** also displayed good recognition of Zn^{2+} over other metal ions except Fe^{2+}, Co^{2+} and Ni^{2+} (Fig. S5b).

3.2. Crystal structures

In order to confirm the structures and binding modes of **1** and **2** with Zn^{2+}, we studied the crystal structures of **1**, **2** and **1**-Zn (Fig. 5). The single crystal X-ray diffraction analysis suggests that all **1**, **2** and **1**-Zn belong to the triclinic space group *P*-1. Detailed crystallographic data are summarized in Table S1.

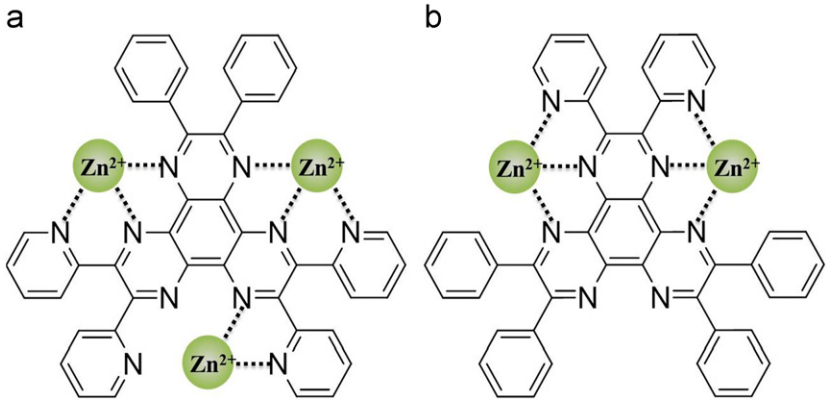

Fig. 4. Proposed binding modes of Zn^{2+} with **1** (a) and **2** (b).

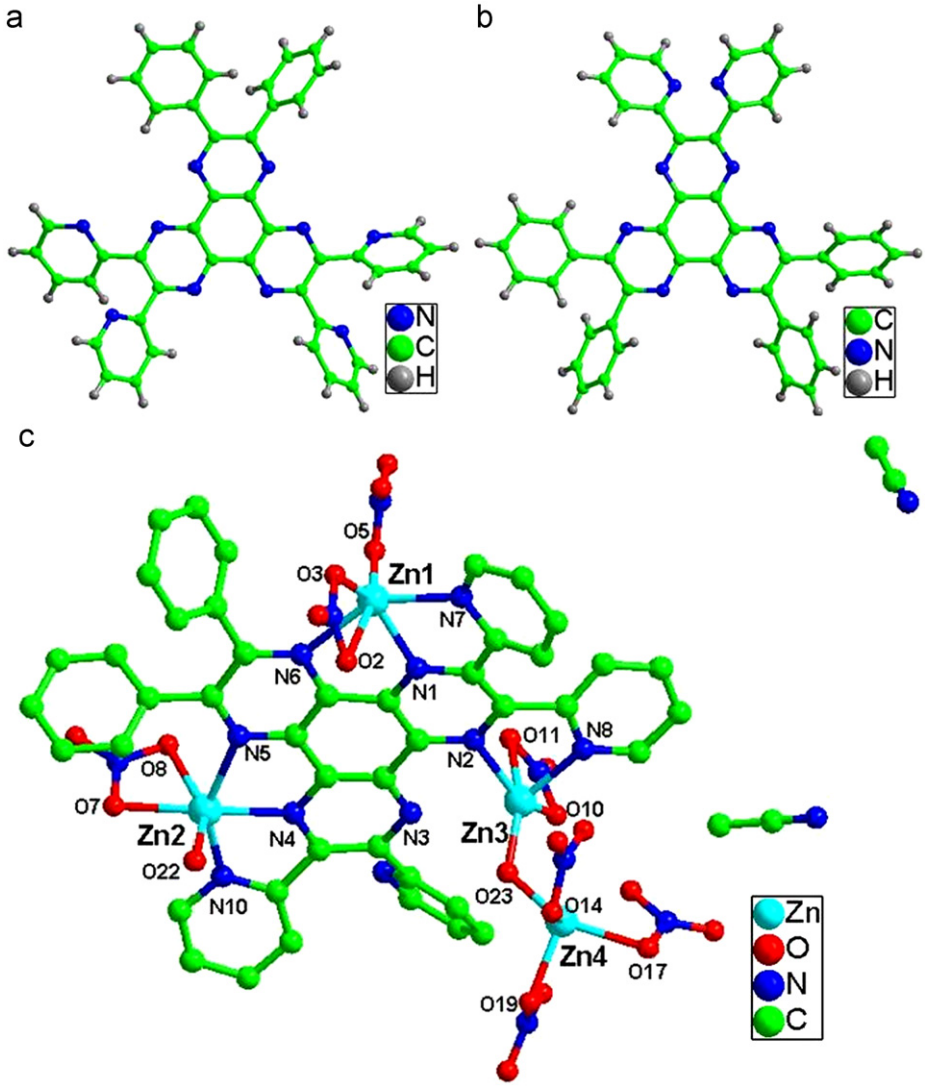

Fig. 5. Crystal structures of **1** (a), **2** (b) and (c).

The single crystal of **1**-Zn is a tetranuclear structure in which **1** coordinates directly to three Zn ions (Zn1, Zn2 and Zn3), while Zn4 is only linked with Zn3 via bridging OH^- (Fig. 5c). Three coordinated pyridyls almost share the same plane with the HAT core owing to the coordination with Zn^{2+} through N7, N8, N10 atoms. Consequently, the coordination of Zn^{2+} enhances the plane rigidity of **1**, and results in the stronger fluorescence effect. The bond lengths of Zn–N/O and the angles of N–Zn–N/ O–Zn–O/ N–Zn–O are listed in Table S2.

As demonstrated before, upon addition of Zn^{2+} ion to **1** in acetonitrile, three Zn^{2+} ions coordinated to one molecule **1**. However, in the crystal state, a tetranuclear structure was obtained.

The different stoichiometries of Zn^{2+} ions to **1** between crystal state and solution state maybe attributed to the requirement of charge balance in the crystal structure. Accordingly, on the base of the single crystal of **1**-Zn, we propose that the structure with 1:3 stoichiometry in acetonitrile is a trinuclear complex of Zn1, Zn2, Zn3 coordinating to one molecule **1** with positive charge (Fig. 5c), which is consistent with the binding modes previously raised (Fig. 4).

3.3. Electronic absorption spectroscopy of *1* and *2*

Normalized absorption spectra of **1** and **2** in acetonitrile (50 μM) are shown in Fig. S6a. The UV–vis spectrum of **1** exhibited three bands around 343, 312, and 249 nm, while **2** showed three absorption bands at 349, 315, and 249 nm. The lowest energy absorption band of **2** red-shifted by 6 nm compared with **1**. The absorption band gaps of **1** and **2**, calculated from the absorption onsets [36], are 3.18 and 3.14 eV (Table 1), respectively, which suggests that the energy gaps of **1** and **2** are extremely close. In contrast to the slight shift of the absorption bands between **1** and **2** in the UV–vis spectra, the corresponding normalized fluorescence spectra of the two compounds displayed almost identical emission bands as shown in Fig. S6b.

The UV–vis titrations of Zn^{2+} to **1** and **2** were also investigated in acetonitrile (Fig. 6). With increasing concentration of Zn^{2+}, two well-defined isosbestic points around 235, 366 nm for **1** and four isosbestic points around 231, 269, 282, 372 nm for **2** appeared in the UV–vis spectra, indicating the formation of new species between Zn^{2+} and **1**, **2**.

3.4. Electrochemical properties of *1* and *2*

The electrochemical properties of **1** and **2** were studied by cyclic voltammetry measurements (Fig. 7), which may shed some light on the interactions between **1** or **2** and the metal ions. The measurement was performed with 10^{-3} M dichloromethane solution using 0.1 M tetrabutylammonium perchlorate as the supporting electrolyte and Ag/AgCl as reference electrode. It is worth mentioning that three reduction waves at −1.27, −1.51, −1.71 V for **1** and −1.34, −1.58, −1.77 V for **2** were observed, which were attributed to the consecutive reduction steps of three pyrazine moieties [18,37,38].

The LUMO energy level was deduced according to the empirical formula $E_{LUMO} = -[4.8 - E_{FOC} + E^{red}_{onset}]$ eV by using the onset potentials for reduction [17,39,40]. The E_{FOC} was the half-wave potential of ferrocene as the standard. As listed in Table 1, the LUMO energy level of **1** was only 0.07 eV lower than that of **2**, which could be negligible. The HOMO energy levels, which were derived from the relationship $E_{gap} = E_{HOMO} - E_{LUMO}$, were calculated to be −6.282 eV for **1** and −6.171 eV for **2**. These results demonstrate that compound **1** has proximate LUMO energy level and energy gap compared with **2**, which may explain the fact that both **1** and **2** exhibit similar electronic absorption and emission behaviors.

Table 1
Electrochemical properties of **1** and **2**.

Compound	E_{onset} (V)[a]	E_{LUMO} (eV)[b]	E_{HOMO} (eV)[d]	E_{gap} (eV)[c]
1	−1.148	−3.102	−6.282	3.18
2	−1.219	−3.031	−6.171	3.14

[a] Obtained from cyclic voltammograms in dichloromethane. Reference electrode: Ag/AgCl.
[b] Calculated from cyclic voltammograms.
[c] Optical band gap.
[d] Calculated according to the formula $E_{HOMO} = E_{LUMO} - E_{gap}$.

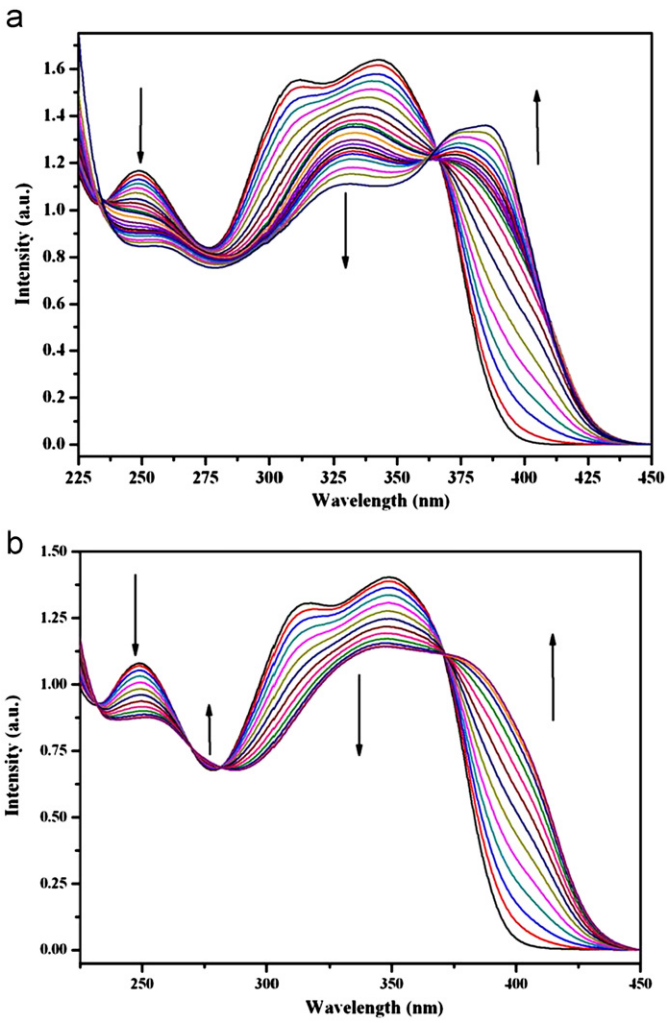

Fig. 6. Absorption spectra of **1** (a) (25 μM) and **2** (b) (25 μM) in the presence of different concentrations of Zn^{2+} in acetonitrile. [(a) 0, 2.5, 5, 7.5, 10, 12.5, 15, 17.5, 20, 22.5, 25, 30, 35, 40, 45, 50, 55, 65, 87.5, 125 μM Zn^{2+}, (b) 0, 2.5, 3.75, 5, 6.25, 7.5, 7.75, 10, 11.25, 12.5, 13.75, 15, 17.5 μM Zn^{2+}].

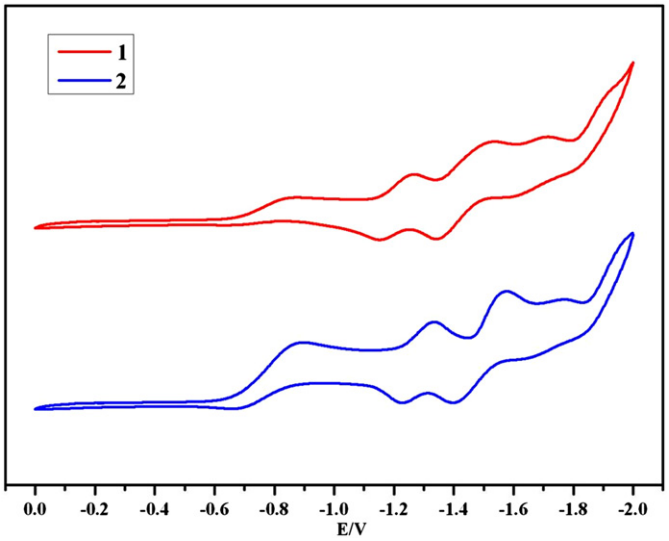

Fig. 7. Cyclic voltammograms of **1** and **2** in dichloromethane at a scan rate of 100 mV/s.

4. Conclusion

We have developed two new C_2-symmetrical HAT derivatives **1** and **2** with different numbers of peripheral pyridine groups. Both of them exhibit ratiometric and colorimetric fluorescence selectivity to Zn^{2+} over alkali ions, alkaline earth ions and a wide range of transition metal ions. Compound **2**, with a detection limit of 0.095 μM, is more sensitive toward Zn^{2+} than **1**. Compound **1** has proximate LUMO energy level, energy gap and coordination sites compared with **2**, which is supported by the optical, electrochemical properties and the single crystal structures of **1**, **2** and **1**-Zn. These results will increase the knowledge of design and applications in fluorescence selectivity for non-centrosymmetric HAT derivatives.

Acknowledgments

This work was supported by the 973 Program (2012CB821700), NSFC (21031002 and 51073079) and the NSF of Tianjin, China (10JCZDJC22100).

Appendix A. Supporting information

Supplementary data associated with this article can be found in the online version at http://dx.doi.org/10.1016/j.talanta.2013.02.071.

References

[1] B.R. Kaafarani, T. Kondo, J. Yu, Q. Zhang, D. Dattilo, C. Risko, S.C. Jones, S. Barlow, B. Domercq, F. Amy, A. Kahn, J.L. Bredas, B. Kippelen, S.R. Marder, J. Am. Chem. Soc. 127 (2005) 16358–16359.
[2] T. Ishi-i, K. Murakami, Y. Imai, S. Mataka, J. Org. Chem. 71 (2006) 5752–5760.
[3] T.H. Chang, B.R. Wu, M.Y. Chiang, S.C. Liao, C.W. Ong, H.F. Hsu, S.Y. Lin, Org. Lett. 7 (2005) 4075–4078.
[4] M. Lehmann, G. Kestemont, R.G. Aspe, C. Buess-Herman, M.H.J. Koch, M.G. Debije, J. Piris, M.P. de Haas, J.M. Warman, M.D. Watson, V. Lemaur, J. Cornil, Y.H. Geerts, R. Gearba, D.A. Ivanov, Chem. Eur. J. 11 (2005) 3349–3362.
[5] S.R. Marshall, A.L. Rheingold, L.N. Dawe, W.W. Shum, C. Kitamura, J.S. Miller, Inorg. Chem. 41 (2002) 3599–3601.
[6] J.R. Galán-Mascarós, K.R. Dunbar, Chem. Commun. (2001) 217–218.
[7] H. Grove, J. Sletten, M. Julve, F. Lloret, J. Chem. Soc. Dalton Trans. (2001) 1029–1034.
[8] Q. Zhao, X.M. Liu, W.C. Song, X.H. Bu, Dalton Trans. 41 (2012) 6683–6688.
[9] D.M. D'Alessandro, M.S. Davies, F.R. Keene, Inorg. Chem. 45 (2006) 1656–1666.
[10] M.G. Fraser, C.A. Clark, R. Horvath, S.J. Lind, A.G. Blackman, X.Z. Sun, M.W. George, K.C. Gordon, Inorg. Chem. 50 (2011) 6093–6106.
[11] Z.Y. Xiao, X. Zhao, X.K. Jiang, Z.T. Li, Chem. Mater. 23 (2011) 1505–1511.
[12] M. Palma, J. Levin, V. Lemaur, A. Liscio, V. Palermo, J. Cornil, Y. Geerts, M. Lehmann, P. Samori, Adv. Mater. 18 (2006) 3313–3317.
[13] B. Liu, Y.F. Ran, Z.Z. Li, S.X. Liu, C.Y. Jia, S. Decurtins, T. Wandlowski, Chem. Eur. J 16 (2010) 5008–5012.
[14] S. Kitagawa, S. Masaoka, Coord. Chem. Rev. 246 (2003) 73–88.
[15] R. Nasielski-Hinkens, M. Benedek-Vamos, D. Maetens, J. Nasielski, J. Organomet. Chem. 217 (1981) 179–182.
[16] Q. Zhao, R.F. Li, S.K. Xing, X.M. Liu, T.L. Hu, X.H. Bu, Inorg. Chem. 50 (2011) 10041–10046.
[17] M. Wang, Y. Li, H. Tong, Y.X. Cheng, L.X. Wang, X.B. Jing, F.S. Wang, Org. Lett. 13 (2011) 4378–4381.
[18] R. Juárez, M. Ramos, J.L. Segura, J. Orduna, B. Villacampa, R. Alicante, J. Org. Chem. 75 (2010) 7542–7549.
[19] R. Juárez, M.M. Ramos, J.L. Segura, Tetrahedron Lett. 48 (2007) 8829–8833.
[20] A. Helal, M.H.O. Rashid, C.H. Choi, H.S. Kim, Tetrahedron 68 (2012) 647–653.
[21] Q. Zheng, S. Chen, Z. Wang, Y. Cui, Talanta 85 (2011) 824–827.
[22] L. Shi, Y. Li, Z.P. Liu, T.D. James, Y.T. Long, Talanta 100 (2012) 401–404.
[23] Y.P. Li, H.R. Yang, Q. Zhao, W.C. Song, J. Han, X.H. Bu, Inorg. Chem. 51 (2012) 9642–9648.
[24] B. Tufan, E.U. Akkaya, Org. Lett. 4 (2002) 2857–2859.
[25] D.Z. Rogers, J. Org. Chem. 51 (1986) 3904–3905.
[26] M.E. Hill, F. Taylor, J. Org. Chem. 25 (1960) 1037–1038.
[27] A.X.S. Bruker, SAINT Software Reference Manual Madison, WI, 1998.
[28] G.M. Sheldrick, NT SHELXTL, Program for Solution and Refinement of Crystal Structures Version 5.1, University of Göttingen, Göttingen, Germany, 1997.
[29] H.M. Wu, P. Zhou, J. Wang, L. Zhao, C.Y. Duan, New J. Chem. 33 (2009) 653–658.
[30] X.Y. Zhou, B.R. Yu, Y.L. Guo, X.L. Tang, H.H. Zhang, W.S. Liu, Inorg. Chem. 49 (2010) 4002–4007.
[31] Z. Xu, K.H. Baek, H.N. Kim, J. Cui, X. Qian, D.R. Spring, I. Shin, J. Yoon, J. Am. Chem. Soc. 132 (2010) 601–610.
[32] F. Qian, C. Zhang, Y. Zhang, W. He, X. Gao, P. Hu, Z. Guo, J. Am. Chem. Soc. 131 (2009) 1460–1468.
[33] T. Jiang, Y.F. Zhao, X.M. Zhang, Inorg. Chem. Commun. 10 (2007) 1194–1197.
[34] S.L. Zheng, J.H. Yang, X.L. Yu, X.M. Chen, W.T. Wong, Inorg. Chem. 43 (2004) 830–838.
[35] A. Ciupa, M.F. Mahon, P.A. De Bank, L. Caggiano, Org. Biomol. Chem. 10 (2012) 8753–8757.
[36] J.W. Wang, J. Wu, Y.M. Chen, H.P. Wang, Y.R. Li, W.S. Liu, H. Tian, T. Zhang, J. Xu, Y. Tang, Dalton Trans. 41 (2012) 12936–12941.
[37] R. Juárez, M.M. Oliva, M. Ramos, J.L. Segura, C. Alemán, F. Rodríguez-Ropero, D. Curcó, F. Montilla, V. Coropceanu, J.L. Brédas, Y. Qi, A. Kahn, M.C. Ruiz Delgado, J. Casado, J.T. López Navarrete, Chem. Eur. J. 17 (2011) 10312–10322.
[38] C.Y. Jia, S.X. Liu, C. Tanner, C. Leiggener, L. Sanguinet, E. Levillain, S. Leutwyler, A. Hauser, S. Decurtins, Chem. Commun. 17 (2006) 1878–1880.
[39] H.P. Shi, J.X. Dai, L. Xu, L.W. Shi, L. Fang, S.M. Shuang, C. Dong, Org. Biomol. Chem. 10 (2012) 3852–3858.
[40] M. Luo, H. Shadnia, G. Qian, X. Du, D. Yu, D. Ma, J.S. Wright, Z.Y. Wang, Chem. Eur. J 15 (2009) 8902–8930.